STEM CELLS TRANSLATIONAL MEDICINE®

TISSUE ENGINEERING AND REGENERATIVE MEDICINE

Endochondral Ossification in Critical-Sized Bone Defects via Readily Implantable Scaffold-Free Stem Cell Constructs

PHUONG N. DANG,[a] SAMUEL HERBERG,[a] DAVOOD VARGHAI,[b] HOOMAN RIAZI,[b] DANIEL VARGHAI,[a] ALEXANDRA MCMILLAN,[c] AMAD AWADALLAH,[d] LAUREN M. PHILLIPS,[a] OJU JEON,[a] MINH K. NGUYEN,[a] NEHA DWIVEDI,[a] XIAOHUA YU,[e] WILLIAM L. MURPHY,[e,f] EBEN ALSBERG[a,g]

Key Words. Regenerative medicine • Bone tissue engineering • Growth factor delivery • Microparticles • Self-assembled sheets • Adult stem cells

Departments of [a]Biomedical Engineering, [c]Pathology, [d]Biology, and [g]Orthopaedic Surgery, Case Western Reserve University, Cleveland, Ohio, USA; Departments of [b]Plastic Surgery, Case Western Reserve University, University Hospitals of Cleveland, Cleveland, Ohio, USA; Departments of [e]Biomedical Engineering and [f]Orthopaedic and Rehabilitation, University of Wisconsin, Madison, Wisconsin, USA

Correspondence: Eben Alsberg, Ph.D., Departments of Biomedical Engineering and Orthopaedic Surgery, Case Western Reserve University, 10900 Euclid Avenue, Cleveland, Ohio 44106, USA. Telephone: 216-368-6425; Fax: 216-368-4969; e-mail: exa46@case.edu

Received May 5, 2016; accepted for publication March 15, 2017; first published June 8, 2017.

1066-5099/2017/$30.00/0

http://dx.doi.org/10.1002/sctm.16-0222

ABSTRACT

The growing socioeconomic burden of musculoskeletal injuries and limitations of current therapies have motivated tissue engineering approaches to generate functional tissues to aid in defect healing. A readily implantable scaffold-free system comprised of human bone marrow-derived mesenchymal stem cells embedded with bioactive microparticles capable of controlled delivery of transforming growth factor-beta 1 (TGF-β1) and bone morphogenetic protein-2 (BMP-2) was engineered to guide endochondral bone formation. The microparticles were formulated to release TGF-β1 early to induce cartilage formation and BMP-2 in a more sustained manner to promote remodeling into bone. Cell constructs containing microparticles, empty or loaded with one or both growth factors, were implanted into rat critical-sized calvarial defects. Micro-computed tomography and histological analyses after 4 weeks showed that microparticle-incorporated constructs with or without growth factor promoted greater bone formation compared to sham controls, with the greatest degree of healing with bony bridging resulting from constructs loaded with BMP-2 and TGF-β1. Importantly, bone volume fraction increased significantly from 4 to 8 weeks in defects treated with both growth factors. Immunohistochemistry revealed the presence of types I, II, and X collagen, suggesting defect healing via endochondral ossification in all experimental groups. The presence of vascularized red bone marrow provided strong evidence for the ability of these constructs to stimulate angiogenesis. This system has great translational potential as a readily implantable combination therapy that can initiate and accelerate endochondral ossification in vivo. Importantly, construct implantation does not require prior lengthy in vitro culture for chondrogenic cell priming with growth factors that is necessary for current scaffold-free combination therapies.
STEM CELLS TRANSLATIONAL MEDICINE *2017;6:1644–1659*

SIGNIFICANCE STATEMENT

Using a scaffold-free high-density stem cell system capable of controlled growth factor delivery from incorporated microparticles, enhanced healing of critical-sized calvarial bone defects via endochondral bone formation was achieved within 4 weeks without the need for long term in vitro culture prior to implantation. The microparticle-based delivery system provides controlled local presentation of growth factors to cells, avoiding the need for expensive and lengthy in vitro culture that requires repeated growth factor supplementation. This work lays the foundation for a rapidly implantable regenerative medicine therapy that accelerates endochondral ossification, the body's natural bone repair process. The modular nature of this system lends itself well to the utilization of different cell types and/or bioactive factors to engineer other complex tissues.

INTRODUCTION

Traditional stem cell-based bone tissue engineering strategies use a biomaterial scaffold seeded with regenerative cells and bioactive signals (e.g., growth factors) to induce healing via intramembranous ossification during which the progenitor cells directly differentiate into osteoblasts to form bone [1]. However, issues with this scaffold-based approach for bone regeneration may hinder its clinical implementation. The presence of scaffolds may greatly interfere with cell-cell interactions, which are necessary for tissue development [2], and their interactions with cells may negatively

alter cell phenotype [3]. Synchronizing scaffold degradation with new tissue formation at the defect site is very challenging and, if not properly achieved, can inhibit cell proliferation, extracellular matrix (ECM) production, remodeling and construct integration, and ultimately compromise the integrity of the newly formed bone [4, 5]. Furthermore, depending on the type of scaffold, chemicals used for scaffold production and/or degradation byproducts may result in cytotoxicity and immunogenicity [6]. Additionally, intramembranous ossification-based approaches often fail in the absence of a functional vascular network, which is necessary to deliver nutrients and oxygen to cells for their survival. Poor blood supply has significantly impeded fracture healing in multiple studies [7–9]. Specifically, acute persistent ischemia has been shown to negatively affect cell viability, proliferation, and differentiation, as well as bridging of femoral defects in mice [9]. Implanted cell-seeded scaffolds that failed to promote rapid ingrowth of a vascular supply resulted in cell death in the interior of the constructs [10, 11] with oxygen deficiency as the likely cause [12]. Therefore, bone repair via intramembranous ossification can be severely limited by the lack of a vascular supply, particularly in the case of critical-sized bone defects and nonunion fractures.

Here, we engineered a scaffold-free system of self-assembled, high-density human mesenchymal stem cell (hMSC) sheets containing growth factor-releasing microparticles that is readily implantable for healing of critical-sized calvarial defects via endochondral ossification. Taking advantage of cells' natural ability to produce a tissue-specific ECM, these scaffold-free constructs are easy to produce by simply mixing the system components and seeding onto Transwell membrane inserts. The cells then coalesce through cell–cell interactions and uniformly incorporate the microparticles. High cell viability is achieved since this self-assembling process does not expose cells to harsh environments that are required for some scaffold-based approaches [13]. The high-density nature of these cell constructs provides a biomimetic environment that supports abundant cell–cell interactions, mimicking MSC condensation during long bone development and fracture healing [14–17]. Additionally, the incorporated biodegradable microparticles provide spatiotemporal control of bioactive signal presentation to regulate cell behavior without adversely interfering with cell–cell interactions. Compared to scaffold-based approaches, these constructs may develop and integrate better in vivo without the complications of matching scaffold degradation rate with new tissue formation.

Endochondral ossification-based strategies to bone tissue engineering are advantageous in that, unlike intramembranous ossification-based approaches, the need to establish a dense vascular network is not immediately required for implant survival and success [18]. During this alternative bone formation pathway, an avascular cartilage template is first produced and then subsequently remodeled into bone [16]. This bone-forming approach eliminates the need to establish an initial vascular network because the lower metabolic needs of chondrocytes enable them to survive in an avascular environment [19, 20]. Importantly, the endochondral ossification process has an intrinsic ability to induce angiogenesis to form a vascular network. The endochondral ossification process produces its own natural ECM scaffold through the formation of a calcified cartilage matrix containing hypertrophic chondrocytes that secrete angiogenic factors to recruit blood vessels to the defect site and osteogenic signals to facilitate its remodeling into bone.

These advantages inspired various attempts in recent years to recapitulate the process of endochondral ossification for bone repair [18, 21, 22]. Successful bone formation has been achieved in subcutaneous mouse models by implanting hypertrophic cartilage constructs that were engineered in vitro. Cells were either seeded on or in biomaterial scaffolds (e.g., type I collagen mesh [23], agarose hydrogel [24], collagen-glycosaminoglycan scaffold [25], PLGA scaffold [26, 27]) or used to form scaffold-free high-density cell constructs (e.g., aggregates [25, 28], sheets [29]) then cultured in chondrogenic media containing either transforming growth factor-beta (TGF-β) 1, 2 or 3 for at least 3 weeks and as long as 12 weeks prior to implantation. Additional culture time with supplements such as hypertrophic and/or osteogenic factors (e.g., dexamethasone, ascorbic acid, β-glycerophosphate, thyroxine, retinoic acid) to promote chondrocyte hypertrophy and/or ossification has also been investigated in these studies [23, 25, 29]. In addition to the ectopic implantation models, endochondral bone tissue engineering has also been demonstrated in orthotopic models. Chondrogenically differentiated MSCs were implanted either on a scaffold [30] or as aggregates [31, 32] into critical-sized femoral defects in rodents, and defect bridging was observed after 8 weeks. While these studies were successful in promoting endochondral ossification, they required at least 3 weeks of in vitro culture to produce hypertrophic cartilage constructs prior to implantation. From a clinical perspective, the long-term culture is not ideal due to the time and high costs involved. Furthermore, the repeated supplementation of inductive factors in the media during the long-term in vitro culture can add to this cost. This mode of growth factor delivery also provides little control over signal presentation, and issues with diffusion may limit construct size and shape, and subsequently the types of defects that can be treated.

We hypothesized that these challenges may be overcome by incorporating microparticles capable of controlled delivery of TGF-β1 and bone morphogenetic protein-2 (BMP-2) within clinically relevant high-density hMSC sheets. hMSCs were used because they are easily accessible, their multipotency is preserved after in vitro expansion and they have the capacity to differentiate into both chondrocytes and osteoblasts [33]. Gelatin microparticles (GM) were designed for localized release of TGF-β1 early within the cell sheets to induce cartilage formation. There have also been reports of hypertrophic chondrocyte marker expression, including collagen type X, alkaline phosphatase (ALP), matrix metalloproteinase-13 (MMP-13), and parathyroid hormone-related protein receptor, during chondrogenic induction with TGF-β [28, 34–36], which is important for endochondral ossification. Mineral-coated hydroxyapatite microparticles (MCM) were engineered for localized delivery of BMP-2 in a more sustained manner to promote chondrocyte hypertrophy [37] and osteogenesis [38] to drive the formation of bone tissue. The microparticle-incorporated hMSC sheet constructs were then implanted to investigate their capacity to heal critical-sized calvarial bone defects in rats. Controlled presentation of chondrogenic and osteogenic signals from microparticles incorporated within hMSC sheets may enhance bone repair via endochondral ossification without the need for a complex scaffold or extended in vitro culture.

Materials and Methods

hMSC Isolation and Expansion

hMSCs were isolated from bone marrow aspirates using a Percoll (Sigma-Aldrich, St. Louis, MO, www.sigmaaldrich.com) density

gradient as previously described [39]. Primary hMSCs were expanded for two passages in media containing low-glucose Dulbecco's modified Eagle's medium (DMEM-LG; Sigma-Aldrich), 10% prescreened fetal bovine serum (ThermoFisher Scientific, Waltham, MA, www.thermofisher.com) and 1% penicillin/streptomycin (ThermoFisher Scientific), and then stored in cryopreservation media in liquid nitrogen until use.

Microparticle Production

GM (average diameter of 60.9 ± 50.1 μm as previously reported [40]) were synthesized with 11.1% wt/vol Type A gelatin from porcine skin (Sigma Aldrich) using a water-in-oil single emulsion technique, cross-linked at room temperature with 1% wt/vol genipin for 2 hours, and characterized as previously described [40–43]. Lyophilized GM were loaded with TGF-β1 (400 ng/mg GM) via incubation in TGF-β1-containing PBS at 37°C for 2 hours.

MCM (average diameter of 3.41 ± 1.04 μm as previously reported [40]) were produced by coating hydroxyapatite microparticles (Plasma Biotal LTD, Derbyshire, UK, www.plasma-biotal.com) via incubation in modified simulated body fluid (mSBF) at 37°C for 7 days with continuous rotation, and characterized as previously described [40, 44]. mSBF was prepared by mixing 141 mM NaCl, 4.0 mM KCl, 0.5 mM $MgSO_4$, 1.0 mM $MgCl_2$, 20.0 mM HEPES, 5.0 mM $CaCl_2$, 2.0 mM KH_2PO_4, and 4.2 mM $NaHCO_3$ in deionized water after which the pH was adjusted to 6.8. To load BMP-2, MCM was incubated in PBS containing BMP-2 (10 μg/mg MCM) at 37°C for 4 hours.

Scaffold-Free Construct Production

Microparticle-incorporated hMSC sheets were produced for both in vitro and in vivo studies. Briefly, passage 3 hMSCs (2×10^6 cells/sheet) were uniformly mixed with GM (1.5 mg/sheet) with or without loaded TGF-β1 (0.6 μg/sheet) and MCM (0.4 mg/sheet) with or without loaded BMP-2 (4 μg/sheet) in a serum-free basal medium. The basal medium consisted of high glucose DMEM (DMEM-HG) with 10% ITS^+ Premix, 100 nM dexamethasone, 37.5 μg/ml L-ascorbic acid-2-phosphate, 1 mM sodium pyruvate, and 100 μM nonessential amino acids. The mixture was then seeded onto the membrane of Transwell inserts (3 μm pore size, 12 mm diameter; Corning, Corning, NY, www.corning.com) and allowed to self-assemble for 2 days.

In Vitro Culture for Promoting Endochondral Ossification

Two-day-old hMSC sheets designated for in vitro analysis ($N = 4$) were cultured in basal medium for an additional 2 weeks followed by 3 weeks in serum-free osteogenic medium. Osteogenic medium consisted of DMEM-HG with 10% ITS^+ Premix, 1 mM sodium pyruvate and 100 μM non-essential amino acids, 100 nM dexamethasone, 0.173 mM L-ascorbic acid-2-phosphate, and 5 mM β-glycerophosphate. This time course was determined to be optimal for partially recapitulating bone formation via endochondral ossification in hMSC aggregates [40]. Groups with empty GM were treated with TGF-β1 (10 ng/ml) exogenously supplemented in basal media during the first 2 weeks of additional culture. Likewise, BMP-2 (100 ng/ml) was added to the osteogenic media for groups with empty MCM. After 5 weeks of culture, constructs were harvested for analysis. Construct thicknesses were measured with a handheld gauge.

Quantitative Reverse Transcription-Polymerase Chain Reaction Analysis

In a separate experiment from the in vivo study, additional hMSC sheets from each group in the in vivo study ($N = 3$/group) were produced for quantitative reverse transcription-polymerase chain reaction (qRT-PCR) analysis after 2 days of culture in basal medium. Harvested sheets were homogenized in TRI Reagent (Sigma-Aldrich) for subsequent total RNA extraction and cDNA synthesis (iScript kit; Bio-Rad, Hercules, CA, www.bio-rad.com). One hundred nanograms of cDNA were amplified in duplicates in each 40-cycle reaction using a Mastercycler (Eppendorf, Hauppauge, NY, www.eppendorf.com) with annealing temperature set at 60°C, SYBR Premix Ex Taq II (Takara Bio Inc., Kusatsu, Shiga, Japan, www.takara-bio.com), and custom-designed qRT-PCR primers (Supporting Information Table S1; Life Technologies, Grand Island, NY, www.lifetechnologies.com). Transcript levels were normalized to GAPDH, and gene expression was calculated as fold-change using the comparative C_T method [45].

Rat Bilateral Calvarial Defect Model

Two days after scaffold-free constructs were prepared and cultured in basal medium, 12-week-old male athymic rats were injected intraperitoneally with a ketamine (40–45 mg/kg) and dexmedetomidine (0.1–0.15 mg/kg) mixture for anesthesia induction. Aerosolized isoflurane (1%–4%) was used for anesthesia maintenance during surgery. Ophthalmic ointment was applied to prevent corneal dessication. A midline sagittal skin incision was made to expose the calvarium. The skin and periosteum were elevated and retracted. Care was taken to keep the periosteum intact. Under saline irrigation, a trephine bur was used to make two circular 5-mm diameter defects on the parietal bone, one on each side of the sagittal suture, without harming the dura matter. The full thickness of the bone was removed, the defect site was cleaned with sterile gauze and saline irrigation, and the defect was filled with half of one microparticle-incorporated hMSC sheet consisting of 1×10^6 cells incorporated with GM (0.75 mg/construct), with or without loaded TGF-β1 (0.3 μg/construct), and MCM (0.2 mg/construct) with or without BMP-2 (2 μg/construct). Each implant was prepared by cutting a whole sheet in half with a sterile spatula. Constructs at this 2-day time point were moldable and thus could completely fill the defect. In animals with the untreated control group, the defect was left empty. The periosteum was sutured over the defects with absorbable vicryl 6-0, and the incision was closed with a continuous suture using vicryl 5-0. After 4 and 8 weeks, animals were euthanized with carbon dioxide. The skullcap was extracted and fixed in 10% neutral buffered formalin for 24 hours at 4°C. After fixation, the samples were placed in 70% ethanol at 4°C until analysis.

Micro-Computed Tomography

Samples were scanned using a Skyscan 1172 micro-computed tomography (micro-CT) scanner (Bruker, Billerica, MA, www.bruker.com) with a 0.5-mm thick aluminum filter at a voltage of 75 kV and current of 100 μA. Data were acquired at an isotropic resolution of 10 μm, rotation step of 0.5°, 360° rotation and frame averaging of 5. Three-dimensional (3D) reconstruction and analysis were performed using NRecon and CTAn software provided by SkyScan. A global threshold range of 90–255 was used. Thresholding was determined by matching the binary images with the original reconstructed images as previously described [46]. As a result,

the reported data may include calcified cartilage and bone of different degrees of maturity. Using CTAn, bone volume/total volume (BV/TV), trabecular number (Tb.N), trabecular thickness (Tb.Th) and trabecular separation (Tb.Sp) were determined in a defined cylindrical region of interest (ROI) (5 mm diameter; 160 slices at 10 μm thickness = 1.59 mm). The chosen thickness of the ROI was larger than the calvaria thickness (~2 times) to account for some newly formed bone that appeared outside the defect region, most likely resulting from some of the constructs shifting after defect closure. Representative 3D images and Tb.Th maps were created using SkyScan's CTVox software. Tb.Th maps were generated from Tb.Th data sets acquired in CTAn.

The extent of bony union and bridging within defects at both time points was determined by following an established scoring guide (Fig. 3A) [47, 48]. Three blinded reviewers separately evaluated the 3D reconstructed micro-CT images for each condition ($N = 5–7$). The scores were averaged for each sample and then averaged for each condition to determine the overall score for each condition.

Histological Analysis

For the first in vitro study, portions of harvested 5-week-old sheets designated for histological analysis ($N = 4$) were fixed in 10% neutral buffered formalin for 24 hours, embedded in paraffin and sectioned at 5 μm thickness. After micro-CT scanning, samples from the animal study ($N = 5–7$) were decalcified in Tris-EDTA buffer (10% EDTA, 0.05 M Tris-HCl, pH 7.4) for 3 days, embedded in paraffin and sectioned at 5 μm thickness. Coronal sections were obtained in the center of the 5 mm defect. Specimens from both in vitro and in vivo studies were deparaffinized and rehydrated with decreasing concentrations of ethanol. In vitro sections were stained with Safranin O/Fast Green and alizarin red S (ARS), while in vivo sections were stained with H&E and Masson's Trichrome (Ventana Medical Systems, Inc., Tucson, AZ, www.ventana.com).

Histomorphometric Analysis of ARS Staining

ImageJ software (1.47v, National Institutes of Health, Bethesda, MD, www.nih.gov) was used to quantify calcium deposition in in vitro sections ($N = 4$) stained with ARS. First, a user-specified global threshold was selected based on visual inspection of stained specimens for use on all samples (*threshold selected in "Lab" colorspace with values in the L* dimension of: min=0; max=230*). The "Lab" colorspace thresholds images on the basis of pixel intensity alone, allowing for selection of all ARS positive staining. Next, the total specimen area was manually outlined and measured as the total ROI. Next, the global threshold was applied to convert all pixels with an intensity greater than or equal to the selected threshold to black. The total area of all black pixels was selected and measured as the total area of ARS staining. ARS-stained area normalized to the ROI was calculated and reported as % ARS staining.

Immunohistochemistry

Immunohistochemistry was performed on sections (N=3-4 for both in vitro and in vivo samples) to examine the amount and distribution of types I, II, and X collagen, osteopontin, and/or osteocalcin as previously described [40]. After rehydration, endogenous peroxidase activity was quenched by incubating samples in a 1:9 solution of hydrogen peroxide and methanol. For antigen retrieval, pronase was used on sections for collagen staining, and citrate buffer was used for osteopontin and osteocalcin staining. Rabbit anti-human type I collagen (human Col I, ab138492; Abcam, Cambridge, UK, www.abcam.com), rabbit anti-human and rat type II collagen (Col II, ab34712; Abcam), rabbit anti-human and rat type X collagen (Col X, ab58632; Abcam), rabbit anti-human and rat osteopontin (OPN, ab8448; Abcam), and rabbit anti-human osteocalcin (OCN, ab93876; Abcam) were used as primary antibodies, and rabbit IgG (Vector Laboratories, Cambridgeshire, UK, www.vectorlabs.com) was used accordingly as a negative control. With the exception of OCN, the Histostain-Plus Bulk kit and aminoethyl carbazole substrate were used according to the manufacturer's instructions (Invitrogen, Carlsbad, CA, www.invitrogen.com) with Fast Green counterstain. OCN staining was processed using a Bond-Max Automated Immunostainer (Leica Biosystems, Buffalo Grove, IL, www.leicabiosystems.com) with Bond Polymer Refine Detection (Leica Biosystems) and hematoxylin counterstain. Slides were mounted with glycerol vinyl alcohol (Invitrogen).

In Situ Hybridization

In situ hybridization to detect human Alu repeat sequences was performed on paraffin-embedded sections ($N = 2–3$) using an ISH iVIEW Blue Plus Detection Kit (Ventana) and a BenchMark ULTRA automated IHC/ISH slide staining system (Ventana). According to the manufacturer's instructions, the Alu Positive Control Probe II was loaded with reagents from the detection kit and accessory reagents including Red Counterstain II onto the reagent tray and placed on the BenchMark ULTRA staining system. The slides were then loaded and the staining run was initiated. Human and rat tissues were used as positive and negative controls, respectively. After staining completed, the slides were dehydrated following the manufacturer's Dehydration Protocol. The slides were mounted with Surgipath MM 24 Mounting Medium (Leica Biosystems). All slides were imaged using an Olympus BX61VS microscope (Olympus Corporation, Tokyo, Japan, www.olympusamerica.com) with a Pike F-505 camera (Allied Vision Technologies, Exton, PA, www.alliedvision.com).

Statistical Analysis

Quantitative data is reported as mean ± standard deviation. Using InStat 3.06 software (GraphPad Software Inc., La Jolla, CA), one-way Analysis of Variance with Tukey's post hoc tests was performed to compare between conditions at each time point and between time points for each condition with $p < .05$ considered significant.

RESULTS

Development of Scaffold-Free hMSC Constructs

Microparticle-incorporated scaffold-free hMSC constructs were developed by first engineering a microparticle-based delivery system for controlled presentation of TGF-β1 and BMP-2 followed by incorporation of the microparticles within high-density hMSC constructs. Our group recently reported on a microparticle-based growth factor delivery system comprised of low-genipin-crosslinked GM capable of early TGF-β1 release and MCM for more delayed and sustained BMP-2 release [40]. Release studies conducted in collagenase-containing PBS revealed that ~60% of loaded TGF-β1 was released from GM within the first 3 hours and 100% was released after 10 days. Collagenase was used because TGF-β1 release is regulated by the enzymatic degradation of GM,

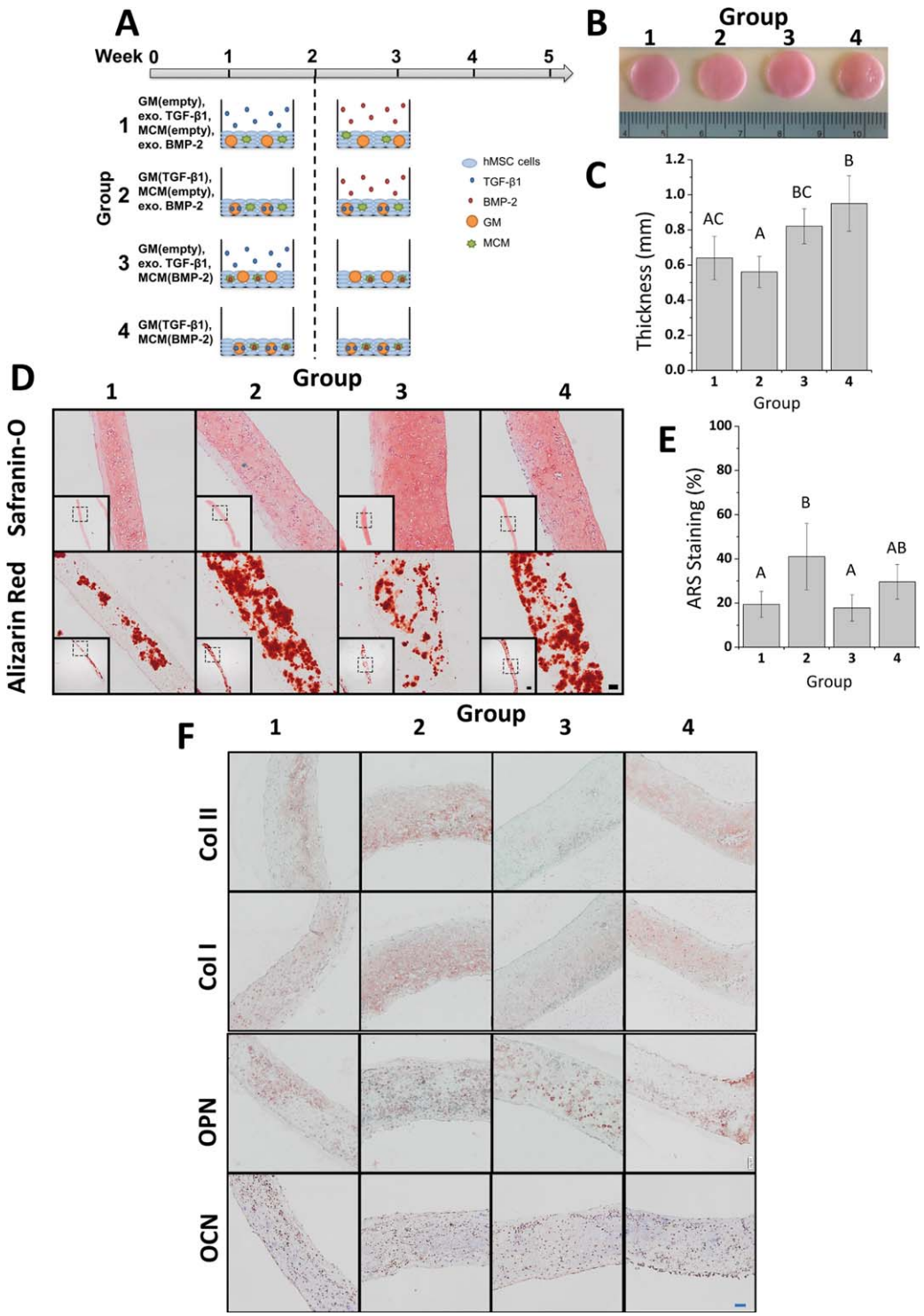

Figure 1. Analysis of scaffold-free hMSC constructs cultured in vitro for 5 weeks. **(A)**: Schematic of conditions. Constructs were incorporated with both GM and MCM that were either left empty or loaded with TGF-β1 or BMP-2, respectively. Each group was cultured for 2 weeks in serum-free basal medium with or without exogenously supplemented (exo.) TGF-β1 and then for 3 weeks in serum-free osteogenic medium with or without exo. BMP-2. **(B)**: Gross images and **(C)**: thickness measurement of constructs after 5 weeks of in vitro culture. Groups that do not share a letter are significantly different at $p < .05$. **(D)**: Photomicrographs of representative Safranin O and ARS stained sections of constructs after 5 weeks of culture. Scale bars = 100 μm, 500 μm (inset). All images are at the same scale. **(E)**: Quantitative analysis of ARS staining. Groups that do not share a letter are significantly different at $p < .05$. **(F)**: Photomicrographs of representative Col II, Col I, OPN, and OCN sections of microparticle-incorporated sheets after 5 weeks of in vitro culture. Scale bar = 100 μm. All images are at the same scale. Abbreviations: ARS, alizarin red S; BMP-2, bone morphogenetic protein-2; Col I, type I collagen; Col II, type II collagen; GM, gelatin microparticles; hMSC, human mesenchymal stem cell; MCM, mineral-coated hydroxyapatite microparticles; OCN, osteocalcin; OPN, osteopontin; TGF-β1, transforming growth factor-beta 1.

which will ultimately be driven by collagenases secreted from cells comprising the constructs. In contrast, BMP-2 was released in a more sustained manner from MCM in PBS with no initial burst, and only ~60% of loaded BMP-2 was released by day 58. Together, these release profiles demonstrate the ability of the microparticle system to deliver TGF-β1 and BMP-2 in a temporally controlled manner to initiate endochondral ossification by first inducing cartilage formation followed by remodeling of the cartilage into bone.

Scaffold-free hMSC constructs were then engineered via the formation of self-assembled hMSC sheets incorporated with the microparticle system using polycarbonate Transwell membrane inserts. The ability of these microparticle-incorporated sheet constructs to partially recapitulate endochondral ossification in vitro was assessed. Four conditions were studied in which all constructs contained both GM and MCM (Fig. 1A). In group 1, constructs were incorporated with empty microparticles that were not loaded with growth factor. In group 2, constructs contained TGF-β1-loaded GM and empty MCM. Group 3 constructs were comprised of empty GM and BMP-2-loaded MCM. Last, constructs in group 4 were incorporated with both GM and MCM loaded with their respective growth factor. Each group was cultured for 2 weeks in serum-free basal medium with or without exogenous TGF-β1 supplemented, and then for 3 weeks in serum-free osteogenic medium with or without exogenous BMP-2. This time course of sequential presentation of soluble signals was determined to best drive endochondral ossification in hMSC aggregates [40]. After 5 weeks, all sheets could be easily manually manipulated and remained intact even after detachment from the Transwell membranes. While group 1 constructs, which were treated with both growth factors exogenously, were softer with smoother surfaces, sheets in groups 2 through 4, which either had one or both growth factors loaded, were palpably stiffer with more uneven surfaces due to the presence of mineralized tissue throughout the constructs (Fig. 1B). These features were most prominent in group 4, in which both growth factors were delivered from the microparticles. Sheets from groups 3 and 4, which contained MCM loaded with BMP-2, were significantly thicker than those in group 2 and groups 1 and 2, respectively, (Fig. 1C).

To evaluate chondrogenesis and tissue mineralization, sections from week 5 constructs were stained for GAG and calcium, respectively (Fig. 1D). Safranin O staining of GAG was observed throughout each construct for all groups. Calcium staining with ARS revealed less staining in groups 1 and 3 compared to groups 2 and 4, which contained TGF-β1-loaded GM and had calcium distributed throughout the constructs. Quantitative analysis of ARS staining confirmed the visual assessment. Relative calcium levels in group 2 were significantly higher compared to groups 1 and 3 ($p < .05$), while levels in group 4 were elevated but did not reach significance (Fig. 1E). Positive staining for types I and II collagen (Col I and II), OPN, and OCN were observed in each group (Fig. 1F). Col II staining was present extensively in groups 1, 2, and 4, with the most intense staining in group 2. Group 3 stained minimally and weakly for Col II. Positive staining for both Col II and GAG (Fig. 1D) confirmed the formation of cartilage within the microparticle-incorporated sheets. Similar to calcium staining, positive staining for Col I was observed throughout in groups 1, 2, and 4 while group 3 exhibited less and weaker staining. Positive staining for OPN and OCN was also observed in each group. Overall, the histological data suggest the formation of mineralized cartilage constructs with large regions of bone-like tissue in all groups.

Growth Factor-Mediated Priming of hMSC Constructs

To characterize the effects of differential growth factor priming on hMSC sheets for implantation (Fig. 2A), gene expression studies were performed after 2 days of in vitro culture in basal medium. Of note, all groups contained both GM and MCM. Growth factor loading caused distinct patterns of genotypic changes in hMSC sheets compared to no growth factor controls (Fig. 2B–2M). hMSC sheets loaded with both TGF-β1 and BMP-2 (group 5) showed significant upregulation of TGF-β1 receptor type I (TGFBRI) mRNA expression relative to no growth factor controls (group 2) and BMP-2-loaded constructs (group 4), while comparable levels were observed with constructs loaded with TGF-β1 (group 3) (Fig. 2B). TGFBRII expression levels were consistent between groups 2–4; however, a significant decrease was seen in group 5 compared to all other groups (Fig. 2C). There were no significant differences in vascular endothelial growth factor receptor II (VEGFRII; Fig. 2D), BMP-2 receptor type IA (BMPRIA; Fig. 2E), or BMPRII (Fig. 2G) mRNA expression in groups 2–5. BMPRIB expression levels were significantly downregulated in groups 3–5 compared to group 2 (Fig. 2F).

Investigation of key genes of the chondrogenic pathway showed significant upregulation in mRNA expression of the chondrogenic marker sex determining region Y-box 9 (SOX9) in groups 3–5 compared to group 2 (Fig. 2H). In addition, expression levels of aggrecan (ACAN) and collagen type 2A1 (COL2A1) were significantly higher in group 5 compared to all other groups (Fig. 2I, 2J). With respect to osteogenic genes, no differences in the expression of Runt-related transcription factor 2 (RUNX2; Fig. 2K) or the late osteogenic marker OCN (Fig. 2M) were found between groups. However, mRNA levels of the early osteogenic marker ALP were significantly increased in group 4 relative to groups 2 and 3, and in group 5 compared to all other groups (Fig. 2L).

Accelerated Healing of Critical-Sized Rat Calvarial Defects by Scaffold-Free hMSC Constructs

To determine the capacity of scaffold-free hMSC sheets with controlled bioactive factor presentation to heal bone defects via endochondral ossification, 5-mm full thickness critical-sized calvarial defects were created in 12-week old athymic rats and implanted with hMSC sheet constructs incorporated with empty microparticles or with microparticles loaded with TGF-β1 and/or BMP-2 (Fig. 2A). Although the experimental hMSC sheets were cultured in serum-free basal medium for 2 days prior to implantation, even at this early stage, they remained intact after removal from the Transwell membrane. Bone regeneration was examined using micro-computed tomography (micro-CT) and histological and immunohistochemical staining for bone and cartilage markers after 4 and 8 weeks.

After 4 weeks, 3D reconstructed micro-CT images showed minimal bone formation on the outer edge of the defect in the sham control (Fig. 3A; group 1). While defects treated with constructs incorporated with empty microparticles (group 2) and constructs loaded with only TGF-β1 (group 3) were filled with new bone by this early time point, the amount of bone was substantially less than in defects treated with constructs with loaded BMP-2 only (group 4) and with both TGF-β1 and BMP-2 (group 5), in which close to complete defect closure was observed.

Scoring of bony bridging and union following an established grading scale (Fig. 3B) revealed significantly higher scores in all groups implanted with the scaffold-free hMSC constructs

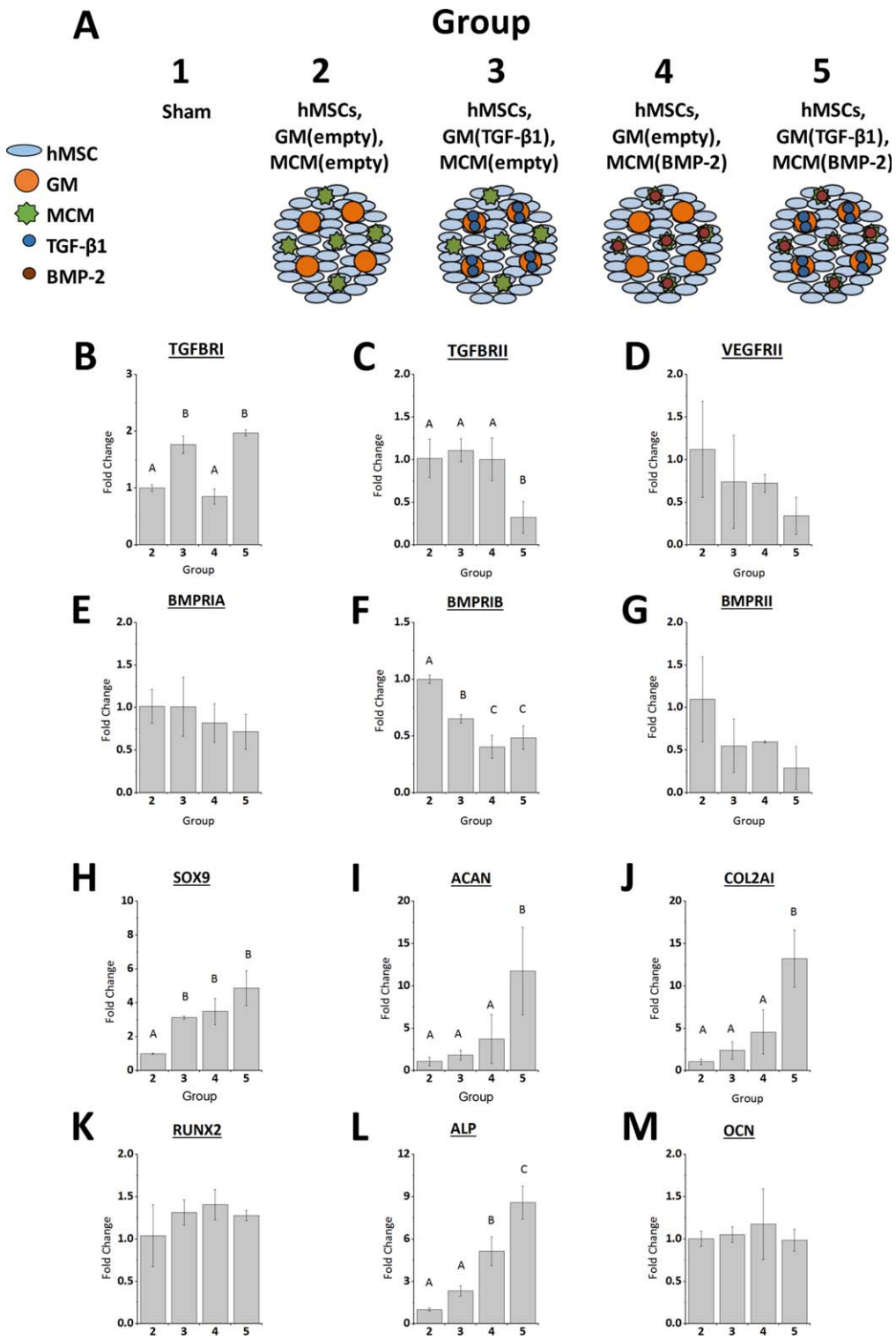

Figure 2. In vivo study conditions and real-time PCR analysis of growth factor receptor expression and cartilage and bone marker expression in day 2 constructs prior to implantation. **(A)**: Schematic of in vivo study conditions. **(B–G)**: Real-time PCR analysis of mRNA expression of (B) TGFBR1, (C) TGFBRII, (D) VEGFRII, (E) BMPRIA, (F) BMPRIB, and (G) BMPRII. **(H–M)**: Real-time PCR analysis of mRNA expression of early and late cartilage markers (H) SOX9, (I) ACAN, (J) COL2A1 and bone markers (K) RUNX2, (L) ALP, and (M) OCN. Groups that do not share a letter are significantly different at $p < .05$. Abbreviations: ACAN, aggrecan; ALP, alkaline phosphatase; BMP-2, bone morphogenetic protein-2; BMPRIA, BMP-2 receptor type IA; BMPRIB, BMP-2 receptor type IB; BMPRII, BMP-2 receptor type II; COL2A1, collagen type 2A1; GM, gelatin microparticles; hMSC, human mesenchymal stem cell; OCN, osteocalcin; RUNX2, Runt-related transcription factor 2; SOX9, sex determining Y-box 9; TGF-β1, transforming growth factor-beta 1; TGFBR1, TGF-β1 receptor type I; TGFBRII, TGF-β1 receptor type II; VEGFRII, vascular endothelial growth factor receptor type II.

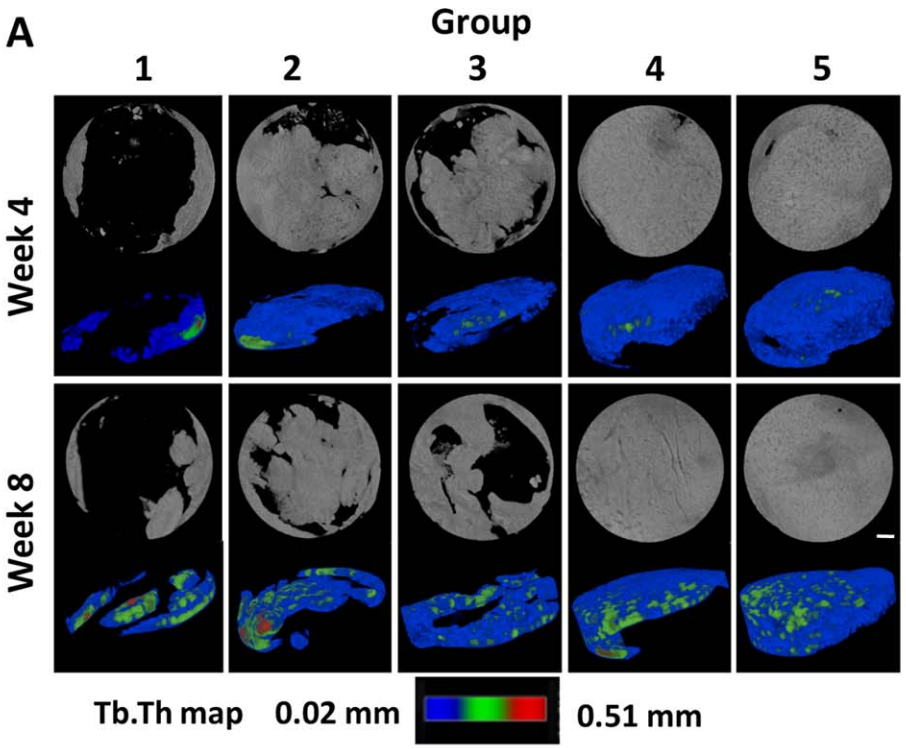

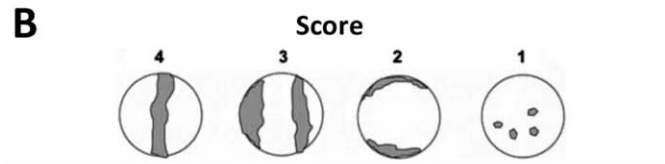

Description	Score
Bony bridging entire span of defect at longest point (5 mm)	4
Bony bridging over partial length of defect	3
Bony bridging only at defect borders	2
Few bony spicules dispersed through defect	1
No bone formation within defect	0

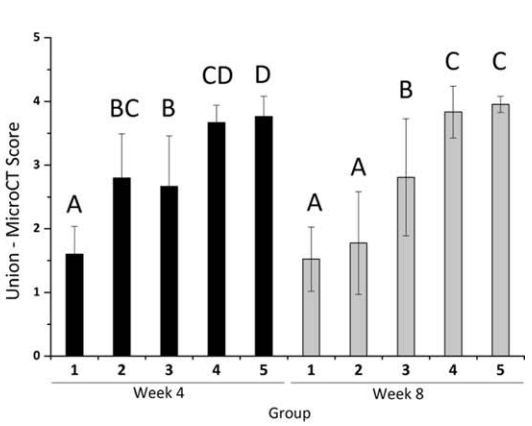

Figure 3. Micro-CT reconstructions of defect regions after 4 and 8 weeks post-implantation and micro-CT scoring for bony bridging and union within defects. **(A)**: Three-dimensional reconstructed micro-CT images **(**top**)** and Tb.Th maps **(**bottom**)** of the defect region in representative samples for each time point. Tb.Th increased from blue to green to red. White scale bar = 500 μm. All images are at the same scale. **(B)**: Scoring guide for extent of bony bridging and union using micro-CT reconstructions (adapted from Patel et al. 2008). **(C)**: Scores for bony bridging and union for the five in vivo groups examined at 4 and 8 weeks. Groups that do not share a letter are significantly different at $p < .05$. Abbreviations: micro-CT, micro-computed tomography; Tb.Th, trabecular thickness.

compared to the sham control, which either showed minimal bony apposition at the defect borders or a few bony spicules within the defect (Fig. 3C). Groups 4 and 5 scored higher for union than group 3. Group 5 further had a significantly higher score than group 2. When BV/TV was measured to determine % healing of the defect, groups 4 and 5 revealed significantly higher BV/TV compared to the other groups at this time point (Fig. 4A). Similarly, Tb.N analysis also showed significantly higher Tb.N in groups 4 & 5 compared to groups 1 through 3 (Fig. 4B). While Tb.Th was similar among all groups (Fig. 4C), Tb.Sp in groups 4 and 5 were significantly lower than group 1, the sham control (Fig. 4D).

At week 8, 3D reconstructed images showed a similar trend among the conditions as week 4 with sham control showing the least amount of new bone tissue formation, and close to complete defect closure in groups 4 and 5 with substantially more bony healing compared with groups 1 through 3 (Fig. 3A). Furthermore, micro-CT scores for union, BV/TV, and Tb.N corroborated the micro-CT images. For these three measures, groups 4 and 5 were significantly higher than groups 1, 2, and 3 (Figs. 3C, 4A, 4B). Group 3 scored significantly higher for union than groups 1 and 2, which scored similarly (Fig. 3C). No significant changes were observed with micro-CT scores and Tb.N from week 4 to week 8 for any group. Importantly, BV/TV significantly increased in group 5 at 8 weeks (Fig. 4A). Further, Tb.Th, significantly increased over time in all groups except group 3 (Fig. 4C). These changes are depicted in the thickness overlay images, which show increasing

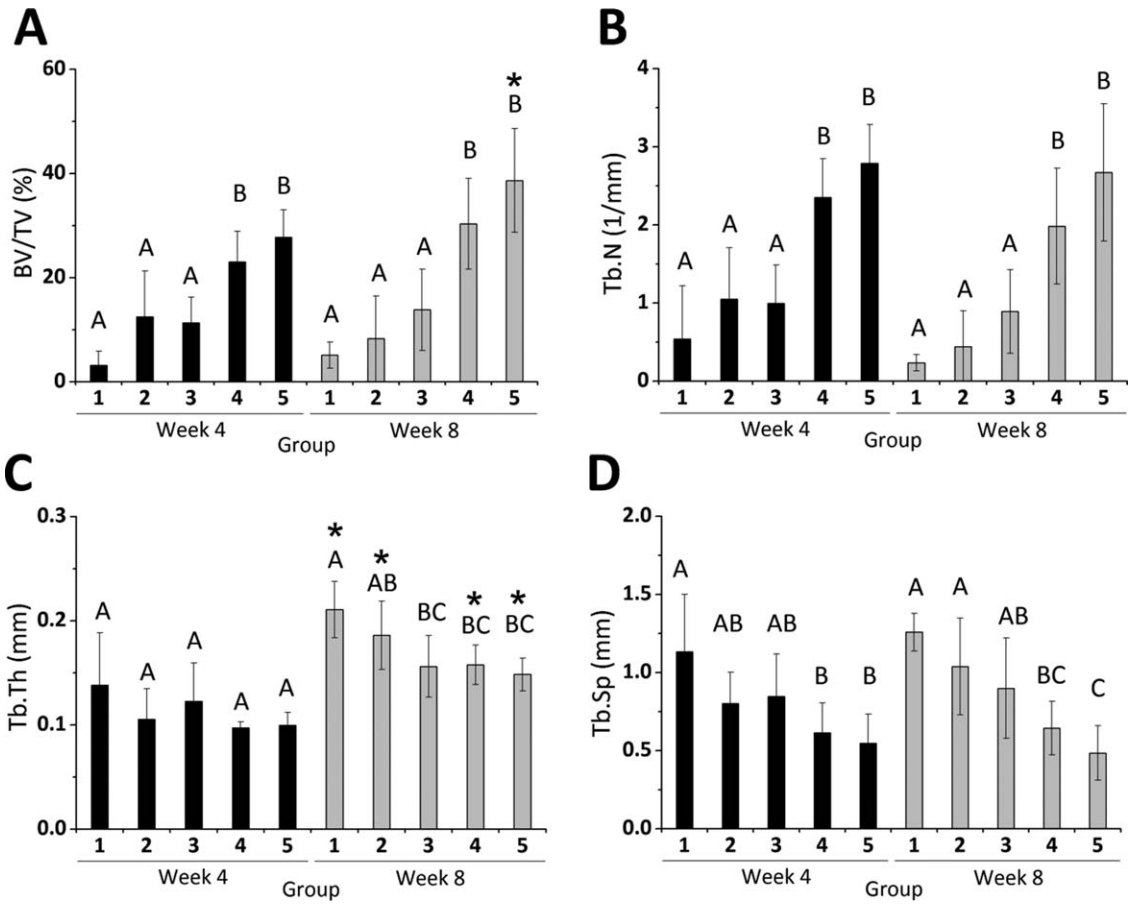

Figure 4. Quantitative micro-computed tomography (micro-CT) analysis. **(A)** BV/TV, **(B)** Tb.N, **(C)** Tb.Th, and **(D)** Tb.Sp of newly formed bone in the defect region at 4 and 8 weeks from micro-CT data. Within each time point, groups that do not share a letter are significantly different at $p < .05$. * Signifies statistical significance compared to week 4. Abbreviations: BV/TV, bone volume/total volume; Tb.N, trabecular number; Tb.Sp, trabecular separation; Tb.Th, trabecular thickness.

thickness from blue to green to red (Fig. 3A). Tb.Sp at week 8 was lowest in groups containing BMP-2-loaded MCM, with groups 4 and 5 being significantly lower than groups 1 and 2 and groups 1 through 3, respectively, (Fig. 4D).

Histological and Immunohistochemical Evaluation of Newly Formed Bone After 4 and 8 Weeks

To evaluate the morphology of the regenerated tissue, decalcified sections were stained with hematoxylin and eosin (H&E) and Masson's trichrome. Photomicrographs at the defect margin and central zone from samples that yielded BV/TV closest to the calculated average for each condition are shown in Figures 5 and 6; complete defect overviews are presented in Supporting Information Fig. S1. At both time points, few bone spicules were embedded in thin cell-rich, fibrous connective tissue spanning the defects in the sham control group with limited new bone originating from the periphery (Figs. 5A, 5a, 6A, 6a; group 1). Defects implanted with scaffold-free hMSC constructs without growth factor loaded (group 2) were partially healed at both time points (Figs. 5B, 6B). New tissue in the defect was comprised of osteoid and woven bone and some more mature lamellar structures with interspersed marrow-like tissue containing blood vessels (Figs. 5B, 5b, 6B, 6b). Similarly, delivering TGF-β1 from GM (group 3) resulted in varying degrees of bone formation that did not completely fill the defects (Figs. 5C, 6C). By week 8, evidence of active remodeling (i.e., presence of lamellar bone) and partially re-established cortical plates was apparent (Figs. 5C, 5c, 6C, 6c). Substantial bone formation with frequent blood vessels and marrow-like tissue was observed as early as week 4 in defects filled with constructs loaded with BMP-2 (Fig. 5D, 5d; group 4) and both BMP-2 and TGF-β1 (Fig. 5E, 5e; group 5). At the latter time point, new bone tissue appeared more extensive in groups 4 and 5 compared to all other groups, with abundant organized lamellar bone containing lacunae-embedded osteocytes (Figs. 6D, 6d, 6E, 6e). At both time points, cortical plates were almost completely re-established achieving defect bridging (Figs. S1D, E, I, J). Importantly, groups 4 and 5 appeared to exhibit a higher degree of vascularization than the other groups, and the marrow spaces in these groups were filled with adipose tissue and/or hematopoietic cells.

To characterize the presence and distribution of human- and/or rat-specific cartilage and bone markers, immunohistochemical staining for human- and rat-specific Col II, human- and rat-specific Col X, and human-specific type I collagen (human Col I) was performed. Regions with the most intense staining for these markers are shown in Figure 7. At week 4, no staining was observed in the sham control for any marker (Fig. 7; group 1). Although limited to small regions throughout each sample, positive staining for Col II and Col X were observed in groups 2, 4, and 5 and groups 2 through 5, respectively. While human Col I staining was observed in groups 2, 4, and 5 at week 4 (Fig. 7C) and groups 4 and 5 at

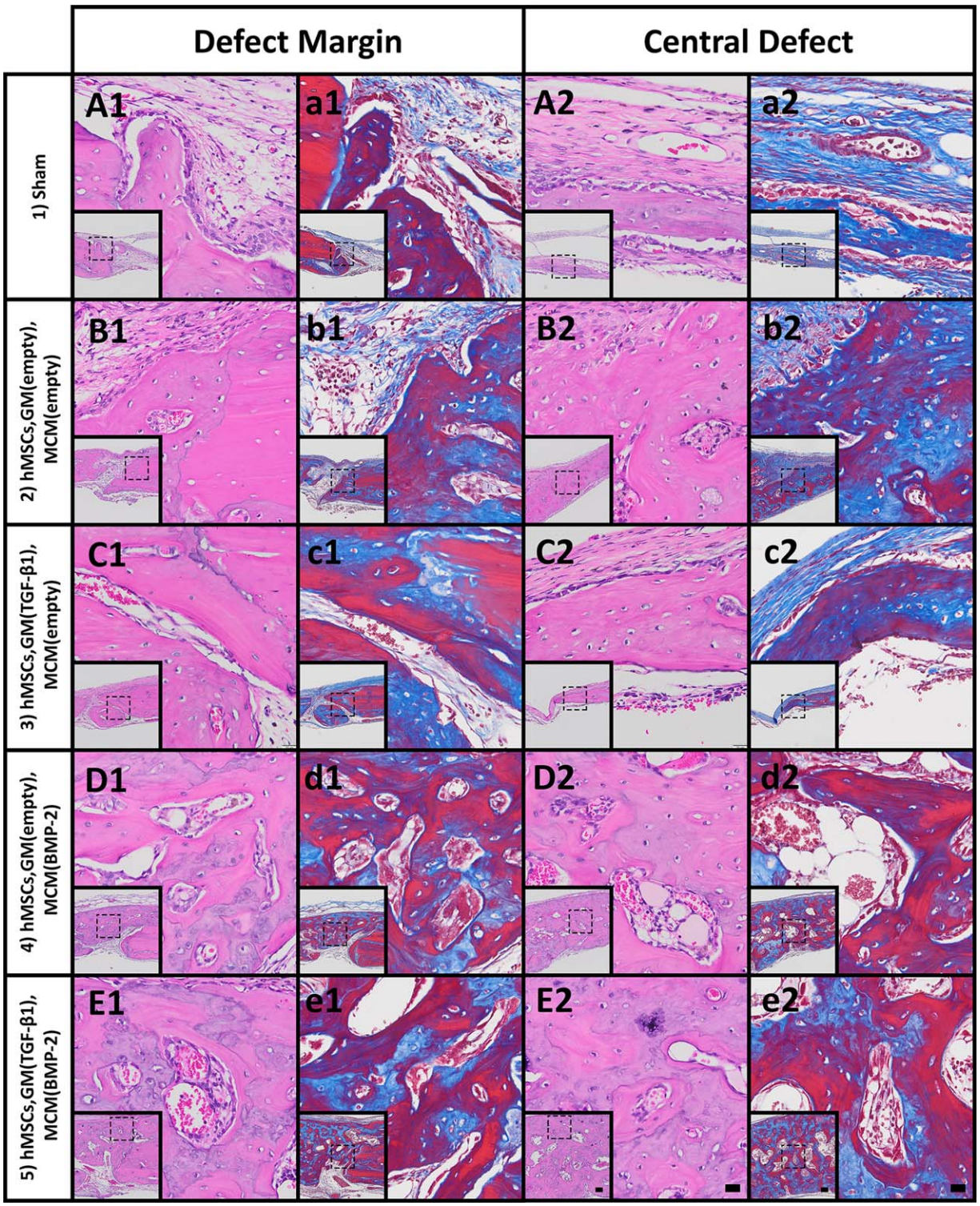

Figure 5. Histological evaluation after 4 weeks. Photomicrographs of **(A1–E1)**: H&E- and **(a1–e1)**: Masson's trichrome-stained sections at the defect margin. Photomicrographs of **(A2–E2)**: H&E- and **(a2–e2)**: Masson's trichrome-stained sections at a central region of the defect. Scale bars = 100 μm (inset), 20 μm (magnification of dotted squares). Abbreviations: BMP-2, bone morphogenetic protein-2; GM, gelatin microparticles; hMSC, human mesenchymal stem cell; MCM, mineral-coated hydroxyapatite microparticles; TGF-β1, transforming growth factor-beta 1.

week 8 (Fig. 7D), staining was minimal throughout each sample. In situ hybridization for human Alu repeats showed some cells of human origin in groups 2, 4, and 5 at week 4 and 3, 4 and 5 at week 8 (Fig. 7E, 7F).

Discussion

Regenerative medicine has emerged as an attractive alternative therapy for treating critical-sized bone defects, which, despite the

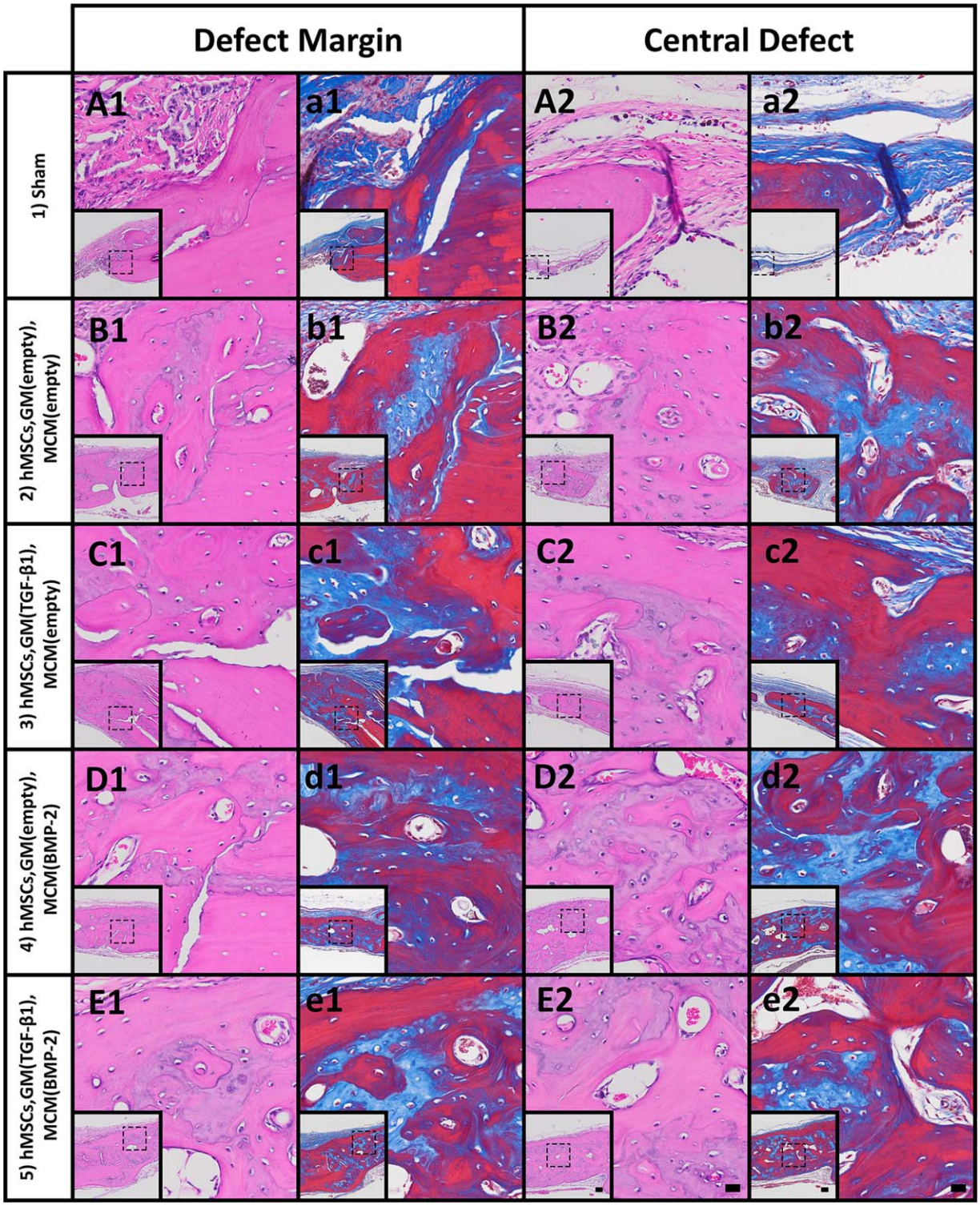

Figure 6. Histological evaluation after 8 weeks. Photomicrographs of **(A1–E1)**: H&E- and **(a1–e1)**: Masson's trichrome-stained sections at the defect margin. Photomicrographs of **(A2–E2)**: H&E- and **(a2–e2)**: Masson's trichrome-stained sections at a central region of the defect. Scale bars = 100 μm (inset), 20 μm (magnification of dotted squares). Abbreviations: BMP-2, bone morphogenetic protein-2; GM, gelatin microparticles; hMSC, human mesenchymal stem cell; MCM, mineral-coated hydroxyapatite microparticles; TGF-β1, transforming growth factor-beta 1.

inherent capacity of bone to repair itself, will not heal in the lifetime of the patient. Bone grafts are the second most common transplant tissue, with 2.2 million transplantations per year at an annual cost of $2.5 billion [1]. Although autografts, the current gold standard, contain essential components for bone regeneration: osteoconductive matrix, osteogenic cells, and osteoinductive factors, transplantation of these grafts may not be possible for large defects due to donor site morbidity and/or limited graft

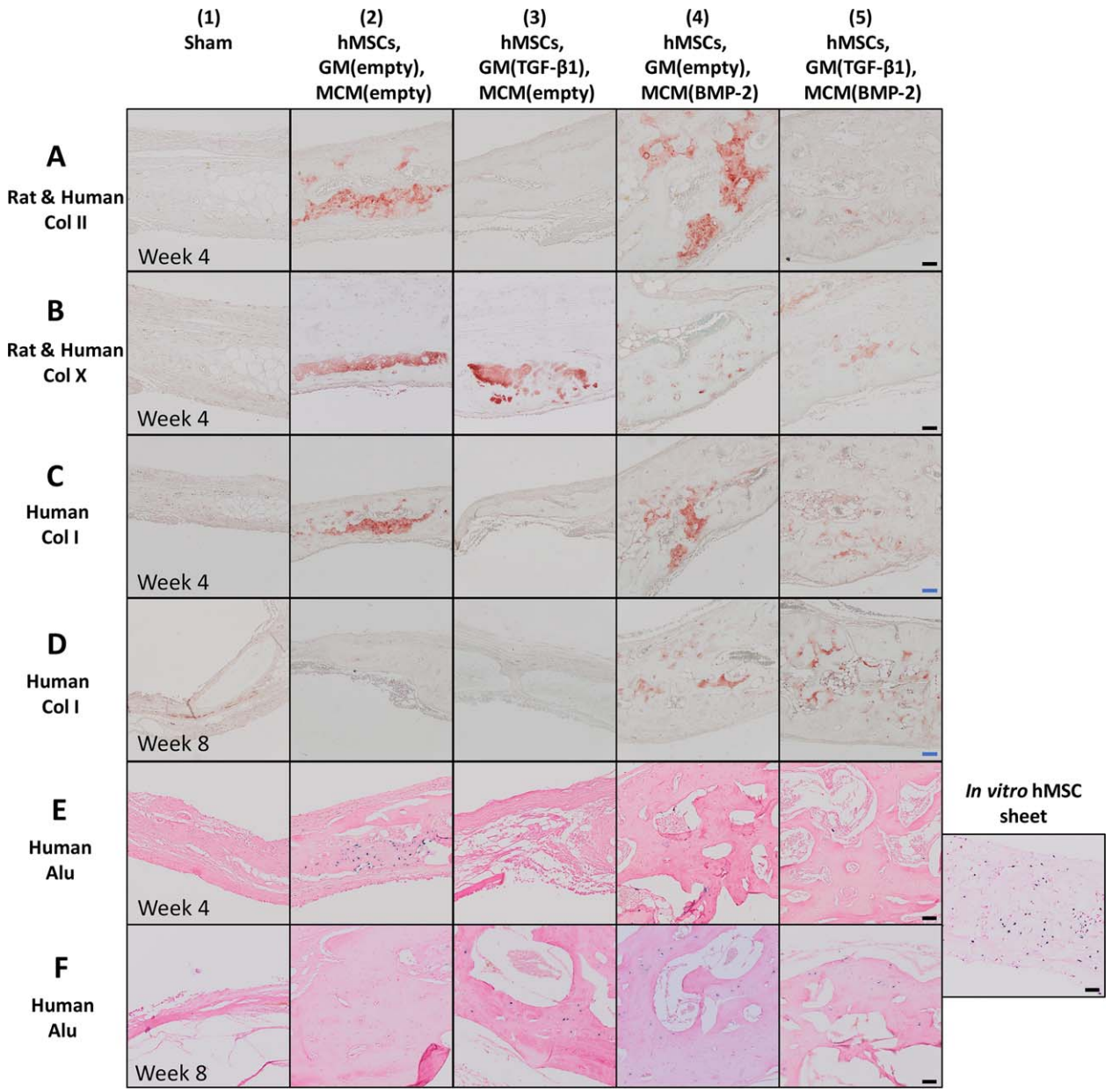

Figure 7. Immunohistological evaluation for extracellular matrix components present in cartilage and bone in the rat calvarial defects at weeks 4 and 8. Photomicrographs of sections at the central defect region stained for **(A)**: human and rat Col II at week 4, **(B)**: human and rat Col X at week 4, **(C)**: human Col I at week 4, and **(D)**: human Col I at week 8. Photomicrographs of human Alu stained sections at the central defect region at **(E)**: week 4 and **(F)**: week 8 and of human Alu staining positive control, a scaffold-free hMSC construct cultured for 5 weeks in vitro. Scale bars = 50 μm (black), 100 μm (blue). Abbreviations: BMP-2, bone morphogenetic protein-2; Col X, collagen X; Col I, type I collagen; Col II, type II collagen; GM, gelatin microparticles; hMSC, human mesenchymal stem cell; MCM, mineral-coated hydroxyapatite microparticles; TGF-β1, transforming growth factor-beta 1.

availability [49–51]. While allografts and xenografts can partially overcome these challenges, they present risks of immune rejection and disease transmission. Treatment with bone morphogenetic proteins (BMPs) delivered from a biomaterial to enhance bone regeneration has been widely used clinically [52, 53], but the high dosage used greatly increases cost and potential for uncontrolled bone growth [54]. These drawbacks have motivated the development of cell-based tissue engineering and regenerative medicine strategies as alternative treatment options. In addition to accelerating and enhancing the regenerative capacity of endogenous cells in the surrounding tissues, delivering cells may provide more refined control over bone growth and lower the dose of codelivered bioactive signal(s) since cells can also secrete their own.

While several tissue engineering systems using scaffold-based strategies have shown promising results in vivo, these approaches face certain challenges that may be difficult to overcome for clinical translation and may hinder their efficacy to heal bone defects [13]. Limitations associated with scaffold-based bone tissue engineering motivated the development of scaffold-free systems that

take advantage of the natural ability of cells to interact with one another, respond to signals and synthesize tissue by secreting their own ECM. Further, the benefits of the high-cell density environment in scaffold-free systems, along with the limitations of the intramembranous ossification approach in promoting vascularized bone formation, steered attempts to engineer bone through the endochondral ossification pathway using the scaffold-free approach. However, scaffold-free systems for endochondral bone formation are not readily implantable because extensive in vitro culture is necessary to prime cells with inductive signals that are often supplemented exogenously in the culture media [25, 28, 29, 31, 32]. In these reported systems, cells were chondrogenically primed for at least 3 weeks prior to implantation.

This work reports the development of a readily implantable scaffold-free hMSC system capable of forming endochondral bone within the body in a controllable manner without the need for an initial vascular supply and extended in vitro culture time. First, self-assembled hMSC sheet constructs with incorporated microparticles capable of controlled delivery of chondrogenic and osteogenic growth factors (e.g., TGF-β1 and BMP-2) were engineered for endochondral bone tissue engineering. An in vitro culture time course of chondrogenic and osteogenic signal presentation to drive osteogenesis of scaffold-free hMSC aggregates in serum-free media was previously identified [40]. Findings from this study demonstrated that the microparticles were able to release TGF-β1 and BMP-2 in a temporally-defined manner to induce formation of more clinically-relevant mineralized sheet constructs that were positive for ECM markers present in bone and cartilage and could serve as a template for endochondral ossification (Fig. 1). Compared to group 1, in which both TGF-β1 and BMP-2 were exogenously delivered, group 4 constructs, which had both TGF-β1 and BMP-2 loaded, were thicker with mineralization occurring throughout the construct (Fig. 1C, 1D). These results indicate the local delivery of TGF-β1 and BMP-2 may result in production of larger cartilage templates with the potential to form larger endochondral bone within the body. Together, these findings provide strong evidence that the microparticles were able to release TGF-β1 and BMP-2 in a temporally-defined manner to induce formation of mineralized constructs that stained positively for both cartilage and bone markers (Fig. 1D, 1F), and could serve as templates for endochondral ossification. Importantly, the controlled, localized delivery of both TGF-β1 and BMP-2 may have enhanced ECM production to form thicker mineralized bone and cartilage constructs during this in vitro culture period.

Members of the TGF-β superfamily, including TGF-β1 and BMP-2, have been shown to facilitate mesenchymal condensation, cell differentiation, and matrix synthesis during cartilage morphogenesis [55–58]. Therefore, gene expression of respective signaling receptors and lineage-specific downstream targets was assessed at day 2 in vitro. TGF-β family ligands signal via hetero-tetrameric receptor complexes comprised of 2 type I receptor components and 2 type II components, both serine/threonine kinases. In the oligomerized complex, type II receptors phosphorylate the type I components, which then activate canonical SMAD signaling [57, 59]. TGF-βs bind type II receptors first followed by recruitment of their type I receptors [60, 61]. Within our study, the observed TGFBR mRNA data at this time point were inconclusive and warrant further investigation (Fig. 2B, 2C). However, significantly downregulated BMPRIB levels with BMP-2 alone or TGF-β1 and BMP-2 (Fig. 2F) indicates potential preferential usage of type IB versus IA receptors upon ligand exposure in this system. This is consistent with the high affinity of BMP-2 for its type I receptors (BMPRIA and IB are functionally redundant during early chondrogenesis) and subsequent ligand-induced receptor downregulation [58, 60, 61]. Presentation of both TGF-β1 and BMP-2 significantly induced mRNA expression of key chondrogenic markers SOX9, ACAN, and COL2A1, while delivery of either growth factor alone only upregulated SOX9 (Fig. 2H–2J), suggesting distinct chondrogenic priming of hMSC sheets at the time of implantation in response to spatiotemporally-controlled morphogen presentation, most notably with TGF-β1 and BMP-2 combined. While early osteogenic gene RUNX2 and late osteogenic marker OCN were largely unaffected by treatment, interestingly ALP expression was upregulated at this early time point in conditions receiving BMP-2 (Fig. 2K–2M), indicating some potential osteogenic priming in these conditions as well.

The capacity of this scaffold-free self-assembled sheet system to facilitate bone formation in vivo was then investigated in a rat bilateral calvarial defect model. Micro-CT analysis and histological evaluation at 4 and 8 weeks revealed that sheet constructs containing growth factor-releasing microparticles cultured for just 2 days were able to rapidly promote healing without prior extended in vitro culture. The sham control (group 1) did not heal within the duration of this study, rendering this defect model critically sized. Partial healing of defects filled with constructs containing hMSCs and unloaded microparticles (group 2) signifies that the presence of hMSCs, GM and MCM was able to stimulate new bone tissue formation without the aid of growth factors. Collagen, the native form of gelatin, and hydroxyapatite are two main ECM components of bone [62] and have both been implicated in enhancing bone formation [63, 64]. This high-density cell construct not only provides a biomimetic milieu that is similar to developing bone through the densely cellular environment, but also one that to some extent mimics the composition of native bone ECM. Therefore, it is not surprising that the growth factor-free constructs stimulated partial healing.

When TGF-β1 was added to the system via controlled, localized delivery from GM (group 3), healing was further improved. Group 3 scored significantly higher for bony bridging and union than group 1 at both time points and group 2 at week 8 (Fig. 3C), but no statistically significant differences among these groups were observed for BV/TV, Tb.N and Tb.Sp at either time point (Fig. 4A, 4B, 4D). In contrast, when constructs were loaded with empty GM and BMP-2-loaded MCM, significantly enhanced bone tissue formation was found at both time points as demonstrated by micro-CT scoring for bony bridging and union, BV/TV, Tb.N, and Tb.Sp (Figs. 3C, 4A, 4B, 4D; group 4). The differential effects of BMP-2 and TGF-β1 may be attributed to their differences in concentrations, release rates and/or roles in hMSC differentiation into osteoblasts and chondrocytes. Not only was TGF-β1 concentration (0.3 μg/defect) lower than BMP-2 concentration (2 μg/defect) resulting in a lower total growth factor dose in group 3 compared to group 4, BMP-2 delivery from MCM was more sustained than TGF-β1 release from GM [40]. Further, TGF-β1 has been reported to play a more prominent role in the early stages of osteoblast differentiation and actually suppresses maturation of osteoblasts during the late phase of differentiation [65]. BMP-2, on the other hand, is a potent osteogenic inducer that can promote osteoblast differentiation through all stages [66]. When TGF-β1 and BMP-2 were both locally delivered from incorporated microparticles (group 5), significantly greater bone regeneration and extent of bony bridging and union were observed at both

time points compared to groups 1 through 3 (Figs. 3C, 4A). Although no significant differences were found with group 4, group 5 was the only group in which BV/TV significantly increased from week 4 to week 8, suggesting significantly greater bone tissue formation may result at later time points compared to the other groups.

In groups implanted with scaffold-free hMSC constructs (groups 2 through 5), histologic analysis suggests endochondral ossification may have occurred. The presence of cartilage tissue was confirmed by staining for rat and human cartilage markers Col II and Col X (Fig. 7A, 7B). Although the antibodies used were not species-specific, positive immunohistochemical staining for Col II in groups 2, 4, and 5 at week 4 revealed the presence of hyaline-like cartilage, the precursor tissue in the endochondral ossification process. Moreover, staining for Col X in groups 2 through 5 provided evidence of hypertrophic cartilage supporting the occurrence of endochondral bone formation [67, 68]. The presence of marrow and blood vessels in the newly formed bone tissue in groups 2 through 5 at both time points (Figs. 5, 6) suggests that the microparticle-incorporated hMSC constructs were able to promote angiogenesis and/or vasculogenesis to form a vascular network within the developing tissue. Since the implanted constructs may have fostered an environment that drives endochondral ossification, it is possible that the hypertrophic chondrocytes arising from this process secreted angiogenic factors (e.g., VEGF) to recruit host blood vessels [16, 69] to the defect site in groups 2 through 5 where endochondral bone formation may have occurred. These blood vessels could then bring in hematopoietic stem cells and osteoprogenitor cells to contribute to formation of the vascularized bone tissue [70, 71].

Human Col I and Alu staining verified the contribution of the implanted hMSCs in bone formation (Fig. 7C–7F). Human Col I staining revealed the presence of bone derived from the implanted hMSCs in some regions of the newly formed tissue (Fig. 7C, 7D). In situ hybridization using the human-specific Alu sequence showed some cells of human origin in defects across groups at both time points (Fig. 7E, 7F). The staining for human markers suggests that the implanted cells may have in part contributed directly to new tissue formation. Several studies have reported the direct participation of MSCs in implanted constructs in bone formation in vivo [23, 29, 32]. Scotti et al. showed that hMSCs implanted subcutaneously either as scaffold-free hypertrophic cartilage constructs [29] or embedded within collagen-based scaffolds [23] after 5 weeks of culture participated in the endochondral ossification process to form ectopic bone in mice. Bahney et al. also reported hMSC pellets that were cultured in vitro for 3 weeks integrated with host bone and directly contributed to fracture healing in a mouse tibia defect model [32].

The portion of the regenerated bone tissue not formed by the transplanted cells must have been derived from rat host cells and likely originated from multiple locations. In a model of nonstabilized tibia fracture healing with an allograft, skeletal progenitor cells from the periosteum gave rise to chondrocytes and osteoblasts that participated in defect repair via endochondral ossification [72]. In contrast, several studies have reported delayed healing when the periosteum is damaged or removed, most likely due to the removal of the local cell source [73, 74]. Given the proximity of the periosteum, which was not removed in this model, it is likely that host periosteal stem cells were recruited to the defects. The implanted hMSCs themselves may have secreted chemoattractants that recruited these host cells [75–77]. Moreover, BMP-2 and/or TGF-β1 delivered from the incorporated microparticles may have aided in this process since these growth factors have been shown to induce chemotaxis of cells in vitro [78, 79] and their roles in recruiting host cells have been implicated during fracture healing [80, 81]. In addition, as previously mentioned, the invading vasculature could also bring in osteoprogenitors. Together, preliminary findings in this report suggest that the implanted constructs provide (a) hMSCs that participate in the regenerative process and (b) trophic signals that recruit progenitor cells to the defect site. Further studies are necessary to determine the relative contributions of host and transplanted cells.

Conclusion

This study demonstrates the utility of a biomimetic tissue engineering approach that partially replicates mesenchymal condensation and activation of specific morphogenetic pathways. To our knowledge, this is the first report of a readily implantable scaffold-free hMSC system featuring presentation of chondro- and osteoinductive growth factors from encapsulated microparticles in a tunable manner for in situ control of cell fate specification capable of enhancing bone healing in a critical-sized defect model. Microparticle-incorporated hMSC constructs implanted only 2 days after production promoted vascularized bone formation as early as 4 weeks. Constructs in which microparticles were loaded with BMP-2 only or TGF-β1 and BMP-2 exhibited significantly increased bridging and BV/TV compared to other groups. Interestingly, BV/TV increased in the dual delivery system from week 4 to week 8, suggesting the potential of delivering TGF-β1 and BMP-2 in a defined manner to strengthen the capacity of the scaffold-free hMSC construct to heal bone defects.

The inclusion of growth factor-releasing microparticles within high-density cultures eliminates the need for external growth factor supplementation and lengthy in vitro culture. The microparticles also provide localized growth factor delivery that allows for production of larger constructs to heal defects of various sizes. Moreover, the moldability of the high-density constructs at the time of implantation enables the treatment of defects of different shapes. Although this work is focused on endochondral bone tissue engineering, the microparticle-incorporated scaffold-free technology may be used for the engineering of other tissue types including skin, cornea, cartilage, meniscus, and vasculature with different combinations of cell types and growth factors. Importantly, the properties of the microparticles (e.g., polymer crosslinking density of GM [42, 43], coating thickness or dissolution rate of MCM [44]) may be modulated to tailor growth factor delivery for other applications. Furthermore, the microparticle approach could also be used in conjunction with the scaffold-free technology for the delivery of other bioactive factors such as anti-inflammatory drugs and genetic material (e.g., DNA, RNA). This platform technology may have wide-ranging versatility for driving the regeneration of bone and other tissues.

Acknowledgments

We thank Ane Garate, Ph.D. and David Wolfson for their contributions to this work. We gratefully acknowledge support from the National Science Foundation Graduate Research Fellowship Program (P.N.D.), the National Institutes of Health (R01AR063194 (E.A.); F32DE024712 (S.H.), and the AO Foundation (W.L.M. and

E.A.). The content is solely the responsibility of the authors and does not necessarily represent the official views of the National Institutes of Health.

Author Contributions

P.N.D.: conception of design, collection and/or assembly of data, data analysis and interpretation, manuscript writing, final approval of manuscript; S.H.: collection and/or assembly of data, data analysis and interpretation, manuscript writing; D.V., H.R., A.A., L.P., O.J., M.K.N., N.D., and X.Y.: collection and/or assembly of data; D.V. and A.M.: collection and/or assembly of data, data analysis and interpretation; W.L.M.: financial support; E.A.: conception of design, data analysis and interpretation, financial support, manuscript writing, final approval of manuscript.

Disclosure of Potential Conflicts of Interest

W.L.M. is cofounder and director of Tissue Regeneration Systems Inc. and cofounder and director of Stem Pharm Inc. The other authors indicated no potential conflicts of interest.

References

1 Meijer GJ, de Bruijn JD, Koole R et al. Cell-based bone tissue engineering. PLoS Med 2007;4:e9.

2 Chen SS, Fitzgerald W, Zimmerberg J et al. Cell-cell and cell-extracellular matrix interactions regulate embryonic stem cell differentiation. Stem Cells 2007;25:553–561.

3 Levy-Mishali M, Zoldan J, Levenberg S. Effect of scaffold stiffness on myoblast differentiation. Tissue Eng Part A 2009;15:935–944.

4 Reis RL, Cohn D. Polymer based systems on tissue engineering, replacement and regeneration. NATO Science Series, Series II: Mathematics, Physics and Chemistry, 1568-2609 86. Dordrecht: Springer Netherlands: Imprint: Springer, 2002:1 online resource (440 pages).

5 Langer RS, Lanza RP, Vacanti J. Principles of Tissue Engineering: Elsevier Inc., 2014: 1 online resource (xlviii, 1887 pages). https://www.elsevier.com/books/principles-of-tissue-engineering/lanza/978-0-12-398358-9

6 Liu X, Ma PX. Polymeric scaffolds for bone tissue engineering. Ann Biomed Eng 2004;32:477–486.

7 Hausman MR, Schaffler MB, Majeska RJ. Prevention of fracture healing in rats by an inhibitor of angiogenesis. Bone 2001;29:560–564.

8 Fang TD, Salim A, Xia W et al. Angiogenesis is required for successful bone induction during distraction osteogenesis. J Bone Miner Res 2005;20:1114–1124.

9 Lu C, Miclau T, Hu D et al. Ischemia leads to delayed union during fracture healing: A mouse model. J Orthop Res 2007;25:51–61.

10 Ishaug-Riley SL, Crane GM, Gurlek A et al. Ectopic bone formation by marrow stromal osteoblast transplantation using poly(DL-lactic-co-glycolic acid) foams implanted into the rat mesentery. J Biomed Mater Res 1997;36:1–8.

11 Ishaug SL, Crane GM, Miller MJ et al. Bone formation by three-dimensional stromal osteoblast culture in biodegradable polymer scaffolds. J Biomed Mater Res 1997;36:17–28.

12 Muschler GF, Nakamoto C, Griffith LG. Engineering principles of clinical cell-based tissue engineering. J Bone Joint Surg Am 2004;86-A:1541–1558.

13 Athanasiou KA, Eswaramoorthy R, Hadidi P et al. Self-organization and the self-assembling process in tissue engineering. Annu Rev Biomed Eng 2013;15:115–136.

14 Fell HB. The histogenesis of cartilage and bone in the long bones of the embryonic fowl. J Morphol 1925;40:417–459.

15 Johnstone B, Hering TM, Caplan AI et al. In vitro chondrogenesis of bone marrow-derived mesenchymal progenitor cells. Exp Cell Res 1998;238:265–272.

16 Mackie EJ, Ahmed YA, Tatarczuch L et al. Endochondral ossification: How cartilage is converted into bone in the developing skeleton. Int J Biochem Cell Biol 2008;40:46–62.

17 Gerstenfeld LC, Cullinane DM, Barnes GL et al. Fracture healing as a post-natal developmental process: Molecular, spatial, and temporal aspects of its regulation. J Cell Biochem 2003;88:873–884.

18 Thompson EM, Matsiko A, Farrell E et al. Recapitulating endochondral ossification: A promising route to in vivo bone regeneration. J Tissue Eng Regen Med 2014;9:889–902.

19 Coyle CH, Izzo NJ, Chu CR. Sustained hypoxia enhances chondrocyte matrix synthesis. J Orthop Res 2009;27:793–799.

20 Schipani E. Hypoxia and HIF-1alpha in chondrogenesis. Ann N Y Acad Sci 2006;1068:66–73.

21 Alsberg E, Anderson KW, Albeiruti A et al. Engineering growing tissues. Proc Natl Acad Sci USA 2002;99:12025–12030.

22 Gawlitta D, Farrell E, Malda J et al. Modulating endochondral ossification of multipotent stromal cells for bone regeneration. Tissue Eng Part B Rev 2010;16:385–395.

23 Scotti C, Piccinini E, Takizawa H et al. Engineering of a functional bone organ through endochondral ossification. Proc Natl Acad Sci USA 2013;110:3997–4002.

24 Sheehy EJ, Vinardell T, Buckley CT et al. Engineering osteochondral constructs through spatial regulation of endochondral ossification. Acta Biomater 2013;9:5484–5492.

25 Farrell E, Both SK, Odorfer KI et al. In-vivo generation of bone via endochondral ossification by in-vitro chondrogenic priming of adult human and rat mesenchymal stem cells. BMC Musculoskelet Disord 2011;12:31.

26 Liu K, Zhou GD, Liu W et al. The dependence of in vivo stable ectopic chondrogenesis by human mesenchymal stem cells on chondrogenic differentiation in vitro. Biomaterials 2008;29:2183–2192.

27 Yang W, Yang F, Wang Y et al. In vivo bone generation via the endochondral pathway on three-dimensional electrospun fibers. Acta Biomater 2013;9:4505–4512.

28 Pelttari K, Winter A, Steck E et al. Premature induction of hypertrophy during in vitro chondrogenesis of human mesenchymal stem cells correlates with calcification and vascular invasion after ectopic transplantation in SCID mice. Arthritis Rheum 2006;54:3254–3266.

29 Scotti C, Tonnarelli B, Papadimitropoulos A et al. Recapitulation of endochondral bone formation using human adult mesenchymal stem cells as a paradigm for developmental engineering. Proc Natl Acad Sci USA 2010;107:7251–7256.

30 Harada N, Watanabe Y, Sato K et al. Bone regeneration in a massive rat femur defect through endochondral ossification achieved with chondrogenically differentiated MSCs in a degradable scaffold. Biomaterials 2014;35:7800–7810.

31 van der Stok J, Koolen MK, Jahr H et al. Chondrogenically differentiated mesenchymal stromal cell pellets stimulate endochondral bone regeneration in critical-sized bone defects. Eur Cells Mater 2014;27:137–148; discussion 148.

32 Bahney CS, Hu DP, Taylor AJ et al. Stem cell-derived endochondral cartilage stimulates bone healing by tissue transformation. J Bone Miner Res 2014;29:1269–1282.

33 Steinert AF, Rackwitz L, Gilbert F et al. Concise review: The clinical application of mesenchymal stem cells for musculoskeletal regeneration: Current status and perspectives. Stem Cells Transl Med. 2012;1:237–247.

34 Sekiya I, Vuoristo JT, Larson BL et al. In vitro cartilage formation by human adult stem cells from bone marrow stroma defines the sequence of cellular and molecular events during chondrogenesis. Proc Natl Acad Sci USA 2002;99:4397–4402.

35 Mueller MB, Tuan RS. Functional characterization of hypertrophy in chondrogenesis of human mesenchymal stem cells. Arthritis Rheumat 2008;58:1377–1388.

36 Mueller MB, Fischer M, Zellner J et al. Hypertrophy in mesenchymal stem cell chondrogenesis: Effect of TGF-beta isoforms and chondrogenic conditioning. Cells Tissues Organs 2010;192:158–166.

37 Leboy PS, Sullivan TA, Nooreyazdan M et al. Rapid chondrocyte maturation by serum-free culture with BMP-2 and ascorbic acid. J Cell Biochem 1997;66:394–403.

38 Luu HH, Song WX, Luo X et al. Distinct roles of bone morphogenetic proteins in osteogenic differentiation of mesenchymal stem cells. J Orthop Res 2007;25:665–677.

39 Haynesworth SE, Goshima J, Goldberg VM et al. Characterization of cells with osteogenic potential from human marrow. Bone 1992;13:81–88.

40 Dang PN, Dwivedi N, Phillips LM et al. Controlled Dual growth factor delivery from

microparticles incorporated within human bone marrow-derived mesenchymal stem cell aggregates for enhanced bone tissue engineering via endochondral ossification. Stem Cells Transl Med 2016;5:206–217.

41 Dang PN, Solorio LD, Alsberg E. Driving cartilage formation in high-density human adipose-derived stem cell aggregate and sheet constructs without exogenous growth factor delivery. Tissue Eng Part A 2014;20:3163–3175.

42 Solorio LD, Vieregge EL, Dhami CD et al. Engineered cartilage via self-assembled hMSC sheets with incorporated biodegradable gelatin microspheres releasing transforming growth factor-beta1. J Control Release 2012; 158:224–232.

43 Solorio LD, Dhami CD, Dang PN et al. Spatiotemporal regulation of chondrogenic differentiation with controlled delivery of transforming growth factor-beta1 from gelatin microspheres in mesenchymal stem cell aggregates. Stem Cells Transl Med 2012;1:632–639.

44 Yu X, Khalil A, Dang PN et al. Multilayered Inorganic microparticles for tunable dual growth factor delivery. Adv Funct Mater 2014; 24:3082–3093.

45 Schmittgen TD, Livak KJ. Analyzing real-time PCR data by the comparative C(T) method. Nat Protoc 2008;3:1101–1108.

46 Bouxsein ML, Boyd SK, Christiansen BA et al. Guidelines for assessment of bone microstructure in rodents using micro-computed tomography. J Bone Miner Res 2010;25:1468–1486.

47 Patel ZS, Young S, Tabata Y et al. Dual delivery of an angiogenic and an osteogenic growth factor for bone regeneration in a critical size defect model. Bone 2008;43:931–940.

48 Spicer PP, Kretlow JD, Young S et al. Evaluation of bone regeneration using the rat critical size calvarial defect. Nat Protoc 2012;7: 1918–1929.

49 Habal MB, Reddi AH. Bone grafts and bone induction substitutes. Clin Plast Surg 1994;21:525–542.

50 Betz RR. Limitations of autograft and allograft: New synthetic solutions. Orthopedics 2002;25:s561–570.

51 Laurie SW, Kaban LB, Mulliken JB et al. Donor-site morbidity after harvesting rib and iliac bone. Plast Reconstr Surg 1984;73:933–938.

52 Schmidmaier G, Capanna R, Wildemann B et al. Bone morphogenetic proteins in critical-size bone defects: What are the options? Injury 2009;40(suppl 3):S39–43.

53 Bishop GB, Einhorn TA. Current and future clinical applications of bone morphogenetic proteins in orthopaedic trauma surgery. Int Orthop 2007;31:721–727.

54 Argintar E, Edwards S, Delahay J. Bone morphogenetic proteins in orthopaedic trauma surgery. Injury 2011;42:730–734.

55 Reddi AH. Bone morphogenetic proteins and skeletal development: The kidney-bone connection. Pediatr Nephrol 2000;14:598–601.

56 Pizette S, Niswander L. BMPs are required at two steps of limb chondrogenesis: Formation of prechondrogenic condensations and their differentiation into chondrocytes. Dev Biol 2000;219:237–249.

57 Shi Y, Massague J. Mechanisms of TGF-beta signaling from cell membrane to the nucleus. Cell 2003;113:685–700.

58 Yoon BS, Ovchinnikov DA, Yoshii I et al. Bmpr1a and Bmpr1b have overlapping functions and are essential for chondrogenesis in vivo. Proc Natl Acad Sci USA 2005;102:5062–5067.

59 Massague J. TGFbeta signalling in context. Nat Rev Mol Cell Biol 2012;13:616–630.

60 Massague J. TGF-beta signal transduction. Annu Rev Biochem 1998;67:753–791.

61 Hinck AP. Structural studies of the TGF-betas and their receptors - insights into evolution of the TGF-beta superfamily. FEBS Lett 2012;586:1860–1870.

62 Clarke B. Normal bone anatomy and physiology. Clin J Am Soc Nephrol 2008; 3(suppl 3):S131–139.

63 Zhou H, Lee J. Nanoscale hydroxyapatite particles for bone tissue engineering. Acta Biomater 2011;7:2769–2781.

64 Ferreira AM, Gentile P, Chiono V et al. Collagen for bone tissue regeneration. Acta Biomater 2012;8:3191–3200.

65 Kasagi S, Chen W. TGF-beta1 on osteoimmunology and the bone component cells. Cell Biosci 2013;3:4.

66 Carreira AC, Alves GG, Zambuzzi WF et al. Bone morphogenetic proteins: Structure, biological function and therapeutic applications. Arch Biochem Biophys 2014;561:64–73.

67 von der Mark K, Kirsch T, Nerlich A et al. Type X collagen synthesis in human osteoarthritic cartilage. Indication of chondrocyte hypertrophy. Arthritis Rheumat 1992;35:806–811.

68 Shen G. The role of type X collagen in facilitating and regulating endochondral ossification of articular cartilage. Orthod Craniofac Res 2005;8:11–17.

69 Yang YQ, Tan YY, Wong R et al. The role of vascular endothelial growth factor in ossification. International journal of oral science. 2012;4:64–68.

70 Karsenty G, Wagner EF. Reaching a genetic and molecular understanding of skeletal development. Dev Cell 2002;2:389–406.

71 Maes C. Role and regulation of vascularization processes in endochondral bones. Calcif Tissue Int 2013;92:307–323.

72 Colnot C. Skeletal cell fate decisions within periosteum and bone marrow during bone regeneration. J Bone Miner Res 2009;24: 274–282.

73 Utvag SE, Grundnes O, Reikeraos O. Effects of periosteal stripping on healing of segmental fractures in rats. J Orthop Trauma 1996;10:279–284.

74 Ozaki A, Tsunoda M, Kinoshita S et al. Role of fracture hematoma and periosteum during fracture healing in rats: Interaction of fracture hematoma and the periosteum in the initial step of the healing process. J Orthop Sci 2000;5:64–70.

75 Vanden Berg-Foels WS. In situ tissue regeneration: Chemoattractants for endogenous stem cell recruitment. Tissue Eng Part B Rev 2014;20:28–39.

76 Ko IK, Lee SJ, Atala A et al. In situ tissue regeneration through host stem cell recruitment. Exp Mol Med 2013;45:e57.

77 Gamblin AL, Brennan MA, Renaud A et al. Bone tissue formation with human mesenchymal stem cells and biphasic calcium phosphate ceramics: The local implication of osteoclasts and macrophages. Biomaterials 2014;35:9660–9667.

78 Fiedler J, Roderer G, Gunther KP et al. BMP-2, BMP-4, and PDGF-bb stimulate chemotactic migration of primary human mesenchymal progenitor cells. J Cell Biochem 2002; 87:305–312.

79 Baek SJ, Kang SK, Ra JC. In vitro migration capacity of human adipose tissue-derived mesenchymal stem cells reflects their expression of receptors for chemokines and growth factors. Exp Mol Med 2011;43: 596–603.

80 Beck LS, Amento EP, Xu Y et al. TGF-beta 1 induces bone closure of skull defects: Temporal dynamics of bone formation in defects exposed to rhTGF-beta 1. J Bone Miner Res 1993;8:753–761.

81 Yu YY, Lieu S, Lu C et al. Immunolocalization of BMPs, BMP antagonists, receptors, and effectors during fracture repair. Bone 2010;46:841–851.

See www.StemCellsTM.com for supporting information available online.